Objectives and Constraints for Transonic Wing Optimization

D.J. Poole *, C.B. Allen †, T.C.S. Rendall‡

Department of Aerospace Engineering, University of Bristol, Bristol, BS8 1TR, U.K.

Consideration of the aerodynamic shape optimization problem definition is presented. An issue with drag minimization is that shocked-free solutions often result which have isolated performance improvements. As such, in this paper, optimizing the range parameter is considered enriched with the operating point as a design variable. A constraint on dimensional lift is therefore required. Analytical treatment of this problem is used to demonstrate that supercritical solutions result providing the lift is above a critical threshold. Also, three-dimensional effects penalise lift coefficient and promote higher optimum Mach numbers. Single- and multi-point optimizations of the NASA CRM wing are considered, inspired by the AIAA ADODG Case 4, as well as a range optimization. A shocked solution is found for the range optimization.

I. Introduction and Background

A generic single-objective optimization problem requires minimizing an objective function, J, which is a function of a vector of D design variables, $\boldsymbol{\alpha}$, subject to a set of inequality, $\mathbf{g}$, and equality, $\mathbf{h}$, constraints. Formally, this is written as:

$$\begin{aligned} \underset{\boldsymbol{\alpha}\in\Re^D}{\text{minimise}} \quad & J(\boldsymbol{\alpha}) \\ \text{subject to} \quad & \mathbf{g}(\boldsymbol{\alpha}) \leq \mathbf{0} \\ & \mathbf{h}(\boldsymbol{\alpha}) = \mathbf{0} \end{aligned} \tag{1}$$

Numerical simulation methods to model fluid flows, called computational fluid dynamics (CFD), are used routinely in aerodynamic design, and can be used to evaluate metrics such as lift or drag. Using a metric such as drag as an objective, with, for example, lift added as a constraint (which are both evaluated numerically,) then adding in a shape deformation scheme that links design variables to surface perturbations, produces an aerodynamic shape optimization (ASO) problem. A numerical optimization algorithm is then used to solve the ASO problem.[1–5] The authors have presented work in this area, with developments such as the domain element method,[6] SVD modes,[7] subdivision surfaces[8] and curvature constraints.[9]

Optimizing for minimum drag is a commonly studied problem. For transonic flow, a substantial source of drag is due to the shock; this causes wave drag and also affects the boundary layer. Eliminating the shock therefore leads to large reductions in the drag of the section, and in inviscid flow, should theoretically lead to a zero drag section. The first published shock-free sections can be traced back to Boerstoel[10] and Nieuwland.[11] Harbeck and Jameson[12] later quantified the front in the Mach-C_L space between where shock-free solutions were and were not able to be obtained. Nowadays, shock-free designs for transonic flows around aerofoils are commonly obtained; for example, of the benchmark cases from the AIAA Aerodynamic Design and Optimization Discussion Group (ADODG) [a] shock-free results are readily available for case 2 (transonic, viscous, drag minimization of RAE2822).[13–17]

*Lecturer. Email: d.j.poole@bristol.ac.uk

†Professor of Computational Aerodynamics. Email: c.b.allen@bristol.ac.uk

‡Senior Lecturer. Email: thomas.rendall@bristol.ac.uk

[a]Details available at https://sites.google.com/view/mcgill-computational-aerogroup/adodg and http://mdolab.engin.umich.edu/content/aerodynamic-design-optimization-workshop

While shock-free solutions produce low-drag at the design point, this performance can be severely local; the off-design performance is often severely compromised. It was proved in the final paper of the trilogy by Morawetz[18] that shock-free aerofoils in transonic flow would have a shock if the freestream Mach number was perturbed. The flow structure for these types of aerofoils tends to be a single shock for an increase in the freestream Mach number and a double shock for a decrease in the Mach number.[19] Hence, using point-design for aerofoil optimization can be problematic. This issue was also considered when designing the NASA supercritical aerofoils; Harris[20] stated *"permitting a weak shock rather than trying to design for a shock-free design point also reduces the off-design penalties usually associated with point design airfoils"*.

Optimising for multiple design points is a common approach to give a performance improvement over a broader operating envelope wherein the individual objectives at each point are weight-summed to produce an overall single objective, for example in.[4,21,22] The solution is, however, highly sensitive to the weights for each design point, though automated weight selection has been proposed as a solution.[23,24] Furthermore, the biggest issue is that the cost of a single objective (and gradient) evaluation is multiplied by the number of points. This makes performing high-fidelity, multi-point optimization on fine numerical grids prohibitively expensive for more than a handful of design points. Drela[25] also pointed out that even multi-point optimization results in point-like performance, and to avoid this the number of chosen operating points should be on the order of the number of design variables. It has been stated that the problem of posing a suitable transonic aerofoil optimization problem is still an open one.[16,26]

In a previous study by the authors,[27] the suitable posing of the aerodynamic optimization problem was considered in the context of transonic aerofoil design. An alternative approach to the construction of the aerodynamic optimization problem, including the choice of design point, design variables, objective function and constraints was considered alongside the conventional single- and multi-point drag minimization problem. Maximization of the Breguet range parameter, ML/D, was introduced, subject to constant non-dimensional wing loading. This design problem is not often studied in aerodynamic optimization, however, examples of it can be found in historical aircraft design. For example, figure 1 (which was constructed using the data in the book of Mair and Birdsall[28b], which itself is a processed form of the data from Hanke and Nordwall[29]) shows the range parameter variation with Mach number for different non-dimensional wing loadings of early variants of the Boeing 747.

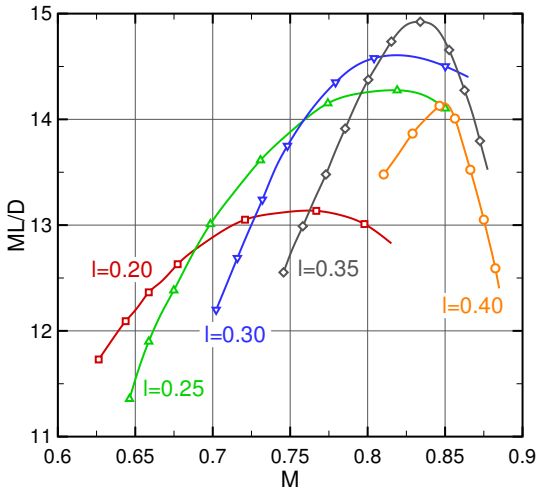

Figure 1: Range variation with Mach number for Boeing 747

Further to considering this design problem, the design point was also considered as a design variable, with Mach number and lift coefficient allowed to vary, however to fully model the trade-offs of speed, lift and drag with range, an induced drag penalty was also introduced.[27] It was shown, both from an analytical treatment and a numerical one, that by considering careful selection of the optimization problem, good on- and off-design results can be achieved by forcing a shocked solution using an optimization problem that is more representative of aircraft design. However, due to considering two-dimensional shapes only, the full trade-offs between speed, range and the aerodynamic forces had to be simulated by the introduction of the

[b]Mair and Birdsall plotted M against D/ML in Figure 10.15, however the inverse is plotted here

induced drag penalty, and this was sufficient to show that the resulting solution was shocked (and therefore lead to more favourable off-design performance). In this paper, the previous work by the authors is extended to investigate three-dimensional wing optimization of range with varying design point subject to constant non-dimensional wing loading.

The investigations in this paper are based on case 4 of the AIAA ADODG, which is single- and multi-point drag reduction of the NASA Common Research Model (CRM) wing. Flow cases defined in case 4 are used, and are compared to range-based optimizations of the wing. The remainder of the paper is organised as follows: section II poses formally the problem studied; section III provides analytical treatment of the problem; section IV describes the aerodynamic shape optimization framework used; section V provides results; finally, conclusions are provided in section VI.

II. Consideration of Range Optimization with Varying Design Point

The majority of transonic aerodynamic optimization seeks to minimise drag at a fixed Mach number, with the consequence that aerofoil geometry is modified to force solutions that are shock-free. As noted in the introduction, shock-free design is well known to degrade off-design behaviour at different Mach number points, as by Morawetz's proof[18] and Drela's demonstrations;[25] a shock-free solution is strongly local. In addition, aircraft design is not driven purely by drag, and an objective that typifies the industrial process more closely is optimizing the range R, which for a cruising, jet-powered aircraft is given by the Brequet range equation:

$$R = \frac{u}{c}\frac{L}{D}\log\left(\frac{W_1}{W_2}\right) \tag{2}$$

where u is the aircraft velocity, c is the specific fuel consumption (SFC), L and D are the lift and drag, and W_1 and W_2 are the initial and final cruise weights respectively. Under the assumption of constant speed of sound through cruise (so $u \propto M$) and constant SFC, the range factor can be extracted, ML/D, which can be used as the objective function in optimization. The equivalent expression using non-dimensional force coefficients is MC_L/C_D. In this scenario, the aerodynamic optimization problem is enriched with the operating point as a design variable. A similar optimization problem has also be considered by Buckley and Zingg,[30] albeit for low-speed UAV design.

Before outlining the final optimization problem, it is worth considering the effect that a varying design point has. A common optimization approach is to constrain C_L, however, this is not suitable in a process where Mach number varies, as equilibrium flight demands a fixed dimensional lift. A more appropriate constraint is therefore $l = M^2 C_L$, which is a non-dimensional measure of wing loading ($\frac{W}{S} = C_L \frac{1}{2}\gamma M^2 P$). This means that when Mach number is a free parameter, the aerofoil is trimmed to achieve the required lift coefficient for that Mach number. The shape is allowed to vary, defined here by a vector, $\mathbf{\Delta x}$, subject to an internal volume (V) requirement to represent the need to house structure or fuel. Hence, the optimization problem is described as:

$$\begin{aligned} \underset{\mathbf{\Delta x}, M}{\text{maximise}} \quad & M\frac{C_L}{C_D} \\ \text{subject to} \quad & M^2 C_L = l \\ & V \geq V_{initial} \end{aligned} \tag{3}$$

In the context of optimization, the cost of solving equation 3 is similar to that of a single-point drag minimization; the addition of Mach number as an extra design variable has little to no effect on the cost. Hence, if multi-point optimization is performed using N design points, then the cost of the single-point and range-based optimization is $O(1/N)$ of the cost of the multi-point.

When solving the range maximization problem for aerofoils previously,[27] an induced drag factor, $C_{D_i} = \kappa C_L^2$ (where $\kappa = 1/\pi AR$ is a constant relating to the aspect ratio) was introduced to model the effect that high lift coefficients would have on the induced component of drag. This had the expected effect of penalising high lift coefficients and resulted in shocked solutions with lower optimal lift but higher optimal Mach. Clearly, it is more ideal to accurately model the effect of aspect ratio and other three-dimensional effects on the optimization results of aerodynamic shapes hence this is the motivation for the current work.

III. Analytical Treatment for Fixed Shape

Before performing geometric optimization, which is presented later, an analytical treatment is considered to find a value of M that optimizes the Breguet range parameter. This involves differentiating the Breguet range parameter with respect to the design variable, which is Mach number. This is performed by first considering inviscid flow, so the only source of drag is due to the shock, as done previously by the authors,[27] and second by introducing an induced drag term. An analytical approximation of wave drag is used to approximate the optimal solution.

A useful (but approximate) analytical result for wave drag is 'Lock's fourth power rule',[31] which may be used to gain insight in to this problem. The premise for this is that drag per unit height of a normal shock scales with $(M - M_c)^3$ (where M_c is the critical Mach number), while the shock height is proportional to $M - M_c$, finally giving a drag proportional to $(M - M_c)^4$. A calibration constant k_w also appears in front of the final result to give a final expression for wave drag, C_{D_w}, as:

$$C_{D_w} = k_w(M - M_c)^4 \tag{4}$$

The physical trade-off for the operating point is very important. At low Mach, lift coefficient must be high. This drives a low critical Mach number and consequently a higher wave drag. At high Mach, the wave drag naturally increases due to the increased offset from M_c. It follows that in between these extremes there lies an optimum where neither the lift coefficient nor Mach number are too high, and it is this optimum that shall be explored with a basic analytical treatment. It has been shown that transonic results arise naturally if M^2C_L is large for the range problem when Mach number is considered in isolation.[27]

The Breguet range parameter is:

$$R = \frac{MC_L}{C_D} \tag{5}$$

Multiplying by M gives a numerator that will differentiate to zero, according to the lift constraint.

$$R = \frac{M^2C_L}{MC_D} \tag{6}$$

Drag is decomposed into wave drag, C_{D_w}, induced drag, C_{D_i}, and the drag due to other effects, C_{D_0}. Wave drag is given by equation 4 and induced drag is given by $k_iC_L^2$, hence equation 6 becomes:

$$R = \frac{M^2C_L}{MC_{D_0} + Mk_w(M - M_c)^4 + Mk_iC_L^2} \tag{7}$$

At the optimum solution, the gradient of the objective with respect to the design variable is zero. To find the optimal Mach, equation 7 (the objective function) is therefore differentiated with respect to M (the design variable), with the result set to zero (noting that M^2C_L is constant so its gradient is zero). For a constraint on l, this leads to:

$$C_{D_0} + k_i\left(C_L^2 + 2MC_L\frac{dC_L}{dM}\right) + k_w(M - M_c)^4 + 4Mk_w(M - M_c)^3\left(1 - \frac{dM_c}{dM}\right) = 0 \tag{8}$$

where:

$$\frac{dC_L}{dM} = -\frac{2MC_L}{M^2} = -\frac{2C_L}{M} = -\frac{2l}{M^3} \tag{9}$$

On the other hand, for a C_L constraint on the range optimization, this leads to:

$$C_{D_0} + k_iC_L^2 + k_w(M - M_c)^4 - 4Mk_w(M - M_c)^3\left(1 - \frac{dM_c}{dM}\right) = 0 \tag{10}$$

Equations 8 and 10 are the resulting polynomials that dictates the optimal condition for the range parameter subject to either l or C_L constraints, and solving allows the optimal Mach number that maximises range to be found. This involves finding M_c and dM_c/dM. The approach to this is given in,[27] for which the reader is guided to for a full description.

In these results, $\left(1 - \frac{dM_c}{dM}\right)$ is typically negative for the M^2C_L case and positive for the C_L case. For the C_L constraint both C_{D_0} and induced drag are constant additions and produce a similar effect, increasing

M_{opt} above M_{crit} as the fourth term in equation 10 becomes more negative to cancel the addition. For the M^2C_L constraint, induced drag penalises lower Mach numbers heavily (and therefore higher C_L values) which pushes M_{opt} up, however C_{D_0} tends to reduce M_{opt} slightly. However, the result will be super-critical above a critical loading value. With this result confirmed, wing optimizations are now presented.

IV. Optimization Framework

In this section, the overall optimization framework used for performing the aerodynamic optimizations outlined later is described. A gradient-based optimizer with a reduced set of design parameters is considered. The geometry and mesh control scheme, optimizer and flow solver are described individually below.

IV.A. Shape Control

The design variables used in the optimization process are the weightings of various sectional deformations. These sectional deformations come about by performing a matrix decomposition that uses SVD on a training library of aerofoils, as proposed by the authors.[32]

IV.A.1. Aerofoil deformations

To obtain aerofoil deformation modes a training library of aerofoils is required[c] In this work, the library of aerofoils is as previously used by the authors for transonic aerofoil optimization.[7] To obtain aerofoil deformation modes, the vector difference between each surface point of all aerofoils is computed. These are combined into an overall deformation matrix $\mathbf{\Psi}$. The deformation matrix has an SVD given by:

$$\mathbf{\Psi} = \mathbf{U}\mathbf{\Sigma}\mathbf{V}^T \tag{11}$$

where $\mathbf{U}$ and $\mathbf{V}$ are orthonormal matrices and $\mathbf{\Sigma}$ is a diagonal matrix with diagonal entries arranged in descending order. The columns of $\mathbf{U}$ contain the aerofoil deformation modes. A subset of deformation modes are extracted and used for optimization. Given the chosen number of deformation modes, D, in the optimization, the design variables are the weightings of each deformation mode. The overall deformation is then a linear superposition of each mode:

$$\mathbf{\Delta X} = \sum_{i=1}^{D} \alpha_i \mathbf{U}_i \tag{12}$$

where α_i is the design variable relating to the i-th mode and $\mathbf{U}_i$ is the i-th mode, the i-th column of $\mathbf{U}$.

IV.A.2. Application to Wing Deformation

The aerofoil deformation modes are surface deformations, however, to ensure body-fitted meshes are retained in the optimization the mesh also needs to deform. Furthermore, the surface deformation modes are applied sectionally, which is defined here.

The sectional deformations are applied at a fixed number of spanwise stations, i.e. equation 12 is applied at these stations locally. The sectional deformations are applied using the RBF control point approach, where a set of control points are defined in the fluid domain and global volume interpolation translates deformation of the control points to deformation of the aerodynamic mesh. Hence, the modal deformations are used to drive deformation of the control points that subsequently deform the wing surface and mesh. These deformations are decoupled, so the control point modal deformations are determined off-line and then applied in the optimization process.

At the heart of this technique in an RBF interpolation developed originally for aero-structure coupling and mesh motion by Rendall and Allen.[33] Control points decouple the shape deformations from the surface mesh and provide a unified framework for surface and mesh deformation. Given n_c control points, a global RBF interpolation of this nature provides exact recovery of data at known sites, and interpolation of that data away from the sites. In the case of optimization, the data to be interpolated is deformation of the control points, hence a deformation field is created. The position of the aerodynamic mesh points in the field

[c]These are obtained from the UIUC database (http://m-selig.ae.illinois.edu/ads/coord_database.html) and are subsequently smoothed and re-parameterised to ensure consistency.

therefore defines the deformation of those points. Since exact recovery of data at the know sites (in this case the position of the control points, which for the j-th control point is defined as $(x_{c_j}, y_{c_j}, z_{c_j})$) is specified, the interpolation takes the form:

$$\Delta \mathbf{x}_c = \mathbf{M}\boldsymbol{\beta}^x$$

where

$$\Delta \mathbf{x}_c = \begin{pmatrix} \Delta x_{c_1} \\ \vdots \\ \Delta x_{c_{n_c}} \end{pmatrix} \qquad \boldsymbol{\beta}^x = \begin{pmatrix} \beta_1^x \\ \vdots \\ \beta_{n_c}^x \end{pmatrix} \qquad \mathbf{M} = \begin{pmatrix} \phi_{1,1} & \cdots & \phi_{1,n_c} \\ \vdots & \ddots & \vdots \\ \phi_{n_c,1} & \cdots & \phi_{n_c,n_c} \end{pmatrix}$$

and analogous definitions hold for the y and z coordinates. The radial basis function $\phi_{i,j} = \phi(\|\mathbf{x}_{c_i} - \mathbf{x}_{c_j}\|)$ can take a number of forms, but the radially-decaying functions of Wendland[34] are a good choice for the mesh deformation problem to give the interpolation a local character and ensure deformation is contained in a region near the moving body. The C^2 function is used here.

Once the linear system is solved, the resulting deformation field can be evaluated at the location of each mesh point. The deformation of an aerodynamic mesh point is given by:

$$\Delta x_a = \sum_{i=1}^{n_c} \beta_i^x \phi(\|\mathbf{x}_{c_i} - \mathbf{x}_a\|) \tag{13}$$

with analogous definitions for y and z.

Using RBF interpolation has the advantage of being able to specify the level of control since control points can be placed arbitrarily in, on the boundary, or outside the fluid domain. The set-up of control points around the CRM wing used in this paper is shown in figure 2.

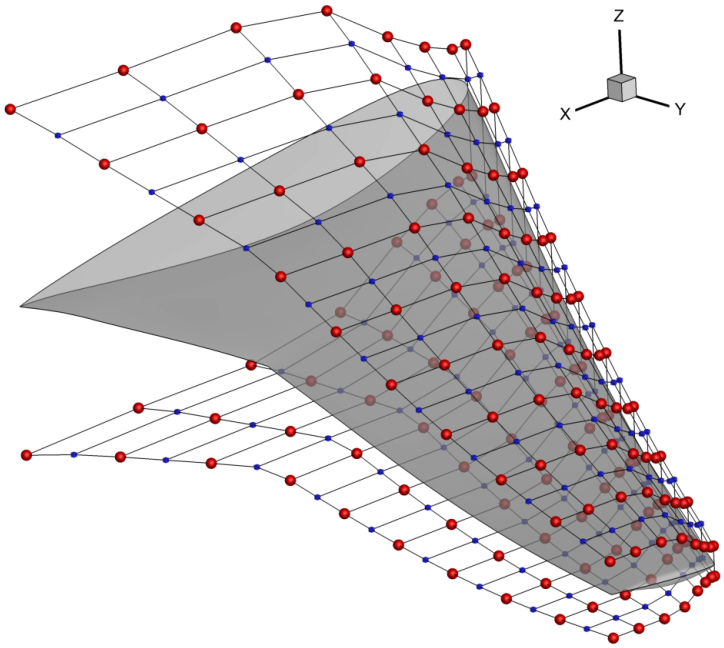

Figure 2: Control point cage around CRM wing

Modal deformations are applied sectionally at ten spanwise station (on the red main control points), while intermediate control points (shown in blue) are used to permit smooth spanwise deformations between the deformation slices.[35] The deformation of intermediate points uses a partition of unity-blend of the deformation slices at either side. A global twist deformation is also introduced. Hence, the sequences of operations is given a set of design variables, $\boldsymbol{\alpha}$, twist deformations of the main sections occurs, followed

by sectional deformations at main spanwise stations. The intermediate sectional deformations are then calculated. Once all control point deformations are defined and calculated, mesh deformation occurs.

IV.B. Optimizer

In the instance considered in this paper, only sectional changes are considered and since fixed planform wing optimization is generally considered to be unimodal (to within numerical tolerances),[36] the gradient-based optimization algorithm, feasible sequential quadratic programming (FSQP) algorithm as implemented in version 3.7,[37] is used. FSQP is based on the sequential quadratic programming (SQP) approach, but modified to improve convergence by combining a search along an arc[38] with a non-monotone procedure for that search.[39] The FSQP algorithm is fully described and analysed in.[40,41]

The gradient-based optimizer requires the sensitivities of the cost and constraint functions with respect to each design variable at each major iteration. For this work, a second-order finite difference stencil is used so for each design variable, two extra flow solutions are required (one each for the positive and negative perturbations) to evaluate the sensitivities. For computational efficiency, a parallel decomposition of the gradient evaluation is employed such that each design design variable sensitivity is assigned to its own CPU, which handles the geometry (and CFD volume mesh) deformations and flow solutions. Once the gradients are evaluated, these are passed back to the master process where the optimizer update occurs.

IV.C. Flow Solver and Meshes

The flow-solver used is a structured multiblock, finite-volume, cell-centred scheme solving the compressible Euler or Reynolds-Averaged Navier-Stokes (RANS) equations in Cartesian and rotating coordinate systems. The convective terms are evaluated using third-order upwind spatial approximation with the flux vector splitting of van Leer.[42] Multi-stage Runge-Kutta with local timestepping is used for time integration, and convergence acceleration is achieved through V-cycle multigrid.[43]

To ensure sufficient aerodynamic resolution, a mesh dependence study is presented. A family of eight-block structured C-meshes (block structure is given in figure 3) was generated using the methods of Allen[44] to give high quality meshes. These range in size from 2.1 million to 0.13 million cells, and are designated L1 (2.1mil), L2 (1.1mil), L3 (580k), L4 (260k) and L5 (130k); sizes were chosen to maximise the number of multigrid levels for each mesh.

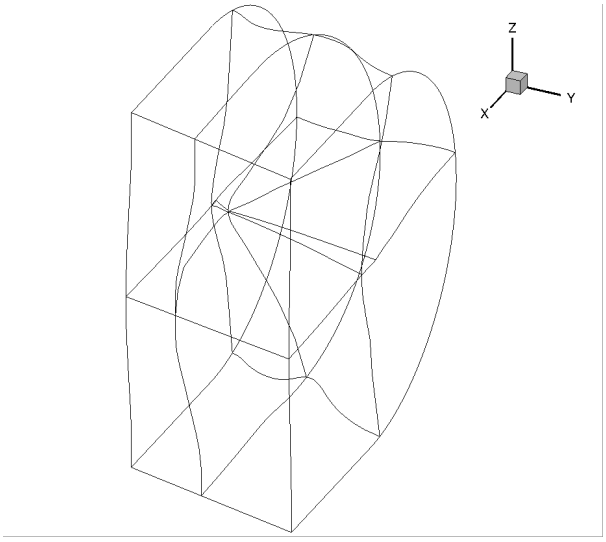

Figure 3: Block structure of eight-block structured C-meshes

Table 1 gives the final drag coefficient on each mesh as well as the run-times as a fraction of the run-time of the coarsest mesh, with the runs being performed in serial to obtain comparable figures. All wings were run at a trimmed cruise C_L of 0.5. Figure 4 gives the surface pressure coefficients of the coarsest and finest meshes. Clearly, there is little difference in the flowfields, but the finer meshes capture the shock more sharply. The L4 mesh, while being relatively coarse, appears to be a good compromise between run-time

and accuracy. This mesh contains 273k nodes and has a 97 × 57 surface mesh, 21 nodes on either side of the wake, and 25 nodes between the inner and outer boundary. Two views of the mesh are shown in figure 5.

Table 1: Force coefficients and run-times (relative to L5 mesh) on different meshes

Mesh	C_L	C_D	Run-time (×L5)
L5	0.5	0.0186	1.0
L4	0.5	0.0156	2.2
L3	0.5	0.0123	4.9
L2	0.5	0.0113	7.2
L1	0.5	0.0110	11.9

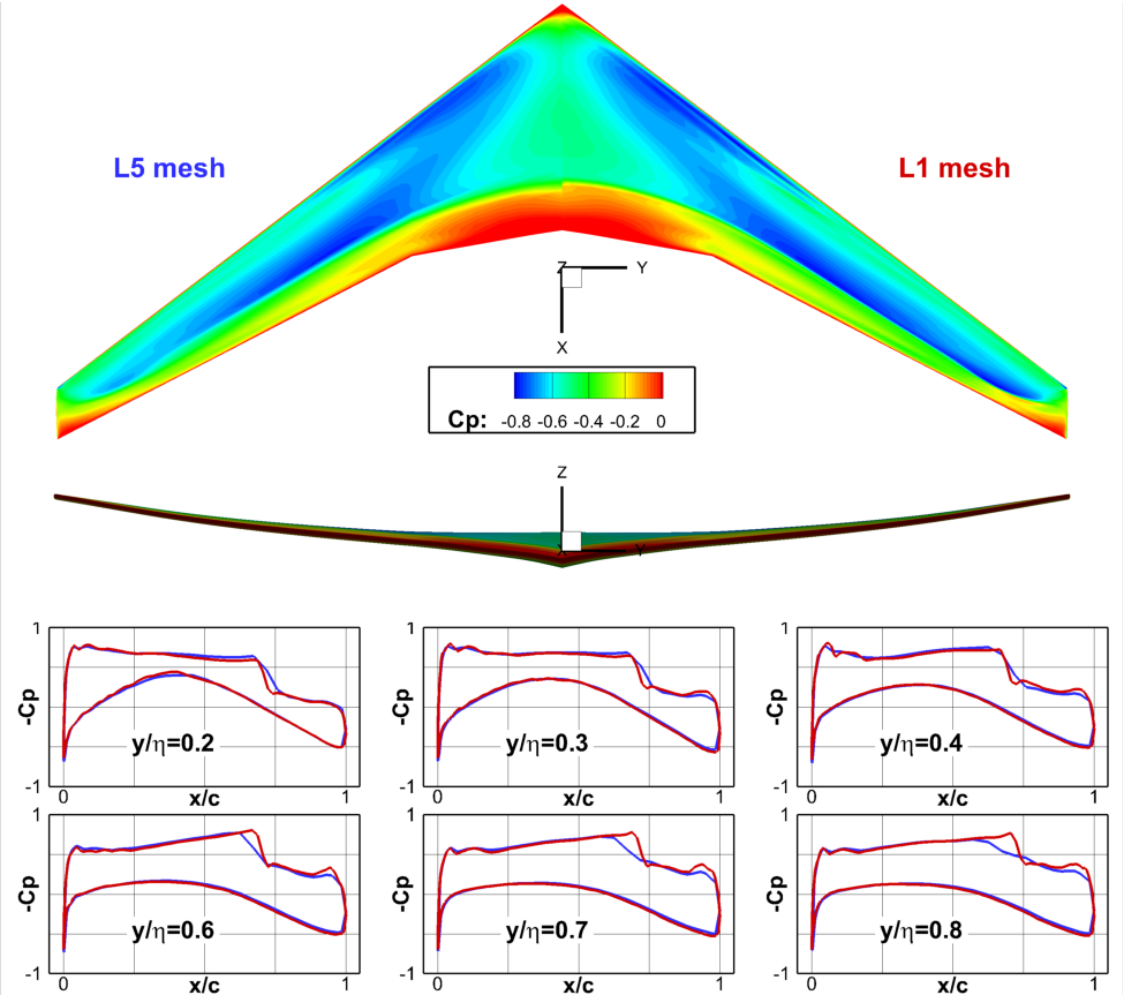

Figure 4: Surface C_P of CRM wing on L5 and L1 meshes

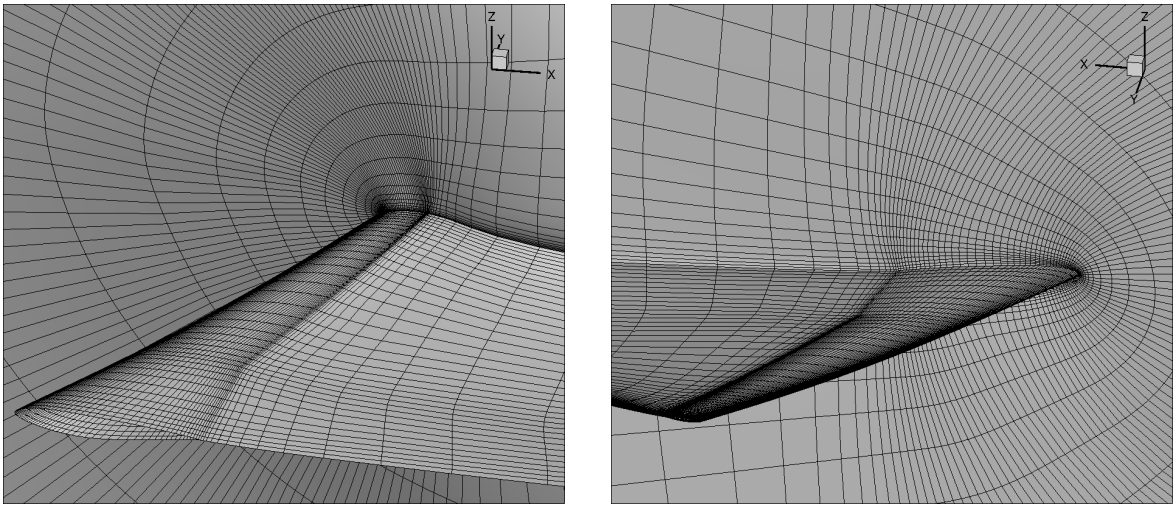

Figure 5: L4 mesh

V. Optimization Results

In this section, single- and multi-point drag minimizations and range optimizations are presented. The optimizations are based on Case 4 of the AIAA ADODG. Case 4.1 defines single-point drag reduction of the CRM wing at a fixed $C_L = 0.5$. This is subject to geometric constraints. It should be noted that the multi-point case definitions have been given different designations in different publications, so for consistency, the reference definitions provided by Nadarajah[d] are used. The case studied here is 4.4 (drag minimization at fixed C_L). Table 2 defines the design points that make up the two cases.

Table 2: Design point definition

Point	M	C_L
a	0.85	0.5
b	0.82	0.5
c	0.88	0.5

In the following definitions of the problems, the superscript refers to the design point designations (a, b and c). The single-point drag-minimization optimization problem is given by:

$$\begin{aligned} \underset{\boldsymbol{\alpha}}{\text{minimise}} \quad & C_D^a \\ \text{subject to} \quad & C_L^a \geq 0.5 \\ & V \geq V_{initial} \end{aligned} \tag{14}$$

The multi-point optimization uses the conventional weighted-sum approach. The sums are defined in the problem definitions. Case 4.4 is given as:

$$\begin{aligned} \underset{\boldsymbol{\alpha}}{\text{minimise}} \quad & \frac{1}{2}C_D^a + \frac{1}{4}C_D^b + \frac{1}{4}C_D^c \\ \text{subject to} \quad & C_L^a \geq 0.5 \\ & C_L^b \geq 0.5 \\ & C_L^c \geq 0.5 \\ & V \geq V_{initial} \end{aligned} \tag{15}$$

[d] https://sites.google.com/view/mcgill-computational-aerogroup/adodg, November 2019

In the range optimization, the design point is allowed to vary but maintaining fixed l, which is given by:

$$\begin{aligned} \underset{\boldsymbol{\alpha}}{\text{maximise}} \quad & M\frac{C_L}{C_D} \\ \text{subject to} \quad & M^2 C_L = l \\ & V \geq V_{initial} \end{aligned} \tag{16}$$

The design variables used for each case are summarised in table 3.

Table 3: Design variable definitions

		Deformation variables		
Problem	Flow variables	Global	Local	Total
Single-point	1 (angle)	1 (twist)	80 (8 modes × 10 sections)	82
Multi-point	3 (angle × 3 points)	1 (twist)	80 (8 modes × 10 sections)	84
Range	2 (angle, Mach)	1 (twist)	80 (8 modes × 10 sections)	83

Given in table 4 are the final results of the single-point case, and in table 5 are the results from the multi-point case. Surface pressure coefficients of the wings are given in figure 6 and 7.

For the single-point case, the expected shock-free solution has resulted at the specified design point. For the multi-point case, the resultant geometry is shock free for design points a and b (the lower Mach numbers) but exhibits a shock at point c. This is a very high cruise Mach number, so is unlikely to be shock-free for any geometry, at least when considered in a multi-point problem where trade-offs of each design point are required. This idea of multi-point being a trade-off is evident when comparing the drag values of point a in cases 4.1 and 4.4, where the multi-point geometry produces slightly higher drag. That being said, both geometries attempt to accelerate the leading edge flow in a smoother manner than the baseline wing, with a gentle pressure recovery to avoid a shock.

Table 4: Results for case 4.1

	C_L	C_D	ΔC_D (%)
Initial	0.5	0.0156	-
Optimised	0.5	0.0146	**-6.4%**

Table 5: Results for case 4.4

Point		C_L	C_D	ΔC_D (%)
A	Initial	0.5	0.0156	-
	Optimised	0.5	0.0149	**-0.7%**
C	Initial	0.5	0.0148	-
	Optimised	0.5	0.0147	**-4.4%**
D	Initial	0.5	0.0210	-
	Optimised	0.5	0.0161	**-23.3%**

For the range optimizations, as already noted, these must be performed at a fixed loading, rather than fixed lift coefficient since Mach is allowed to vary. The loading that matches design point c is considered. This case was started from $M = 0.85$ with C_L trimmed to give the required l.

Table 6 gives the result of the range optimization. Range has been improved over the baseline wing. As found when considering the analytical problem, a high Mach number with lower C_L is preferred over lower

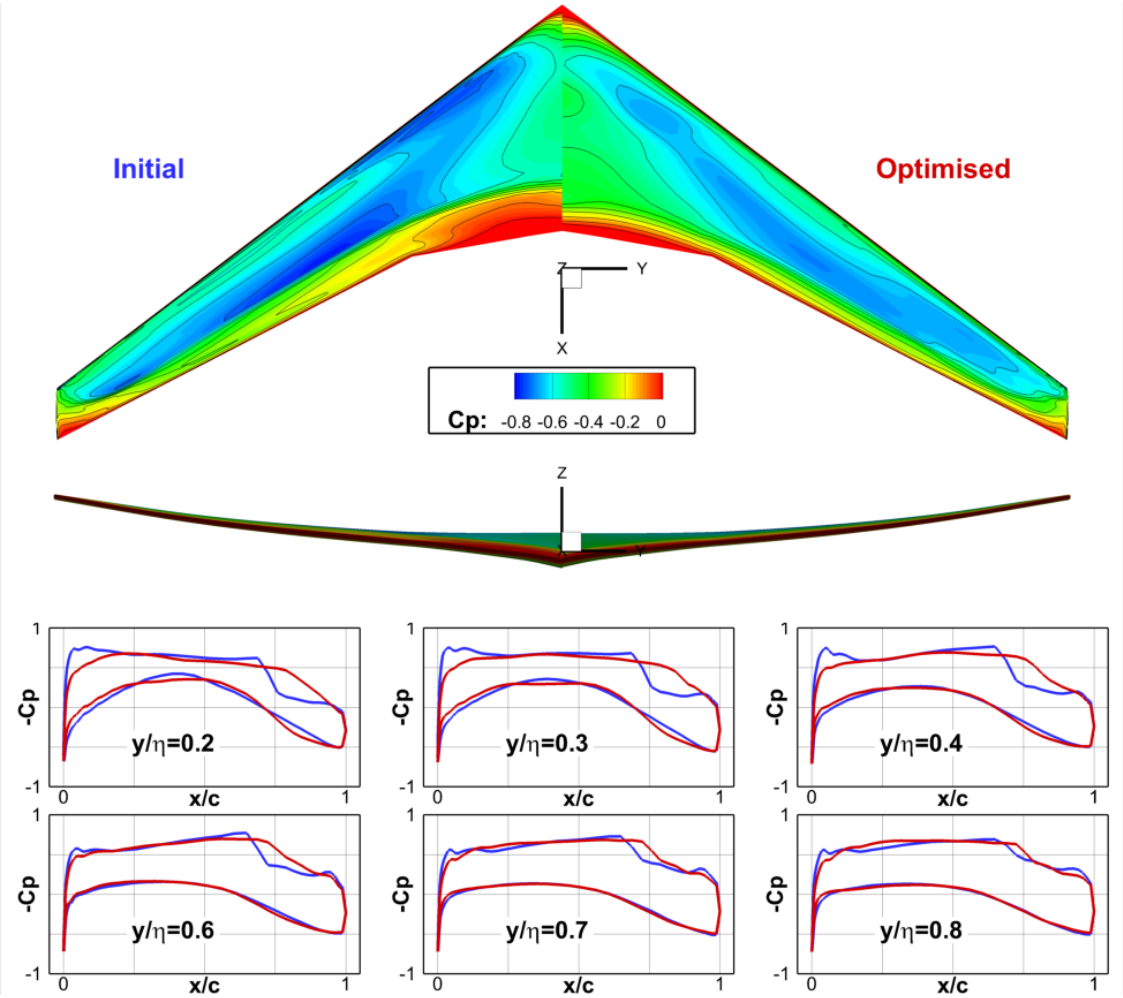

Figure 6: Surface C_P of initial and optimized geometry for case 4.1

Mach numbers.

Table 6: Results for range optimization

	C_L	C_D	M	R
Initial	0.55	0.0185	0.850	25.3
Optimized	0.52	0.0167	0.875	27.2

Figure 8 gives detail surface pressures. The optimization clearly exhibits a shocked solution. Therefore, it appears that the behaviour exhibited in the aerofoil optimizations[27] of high Mach number shocked aerofoils for these type of optimizations, is also repeated for wings.

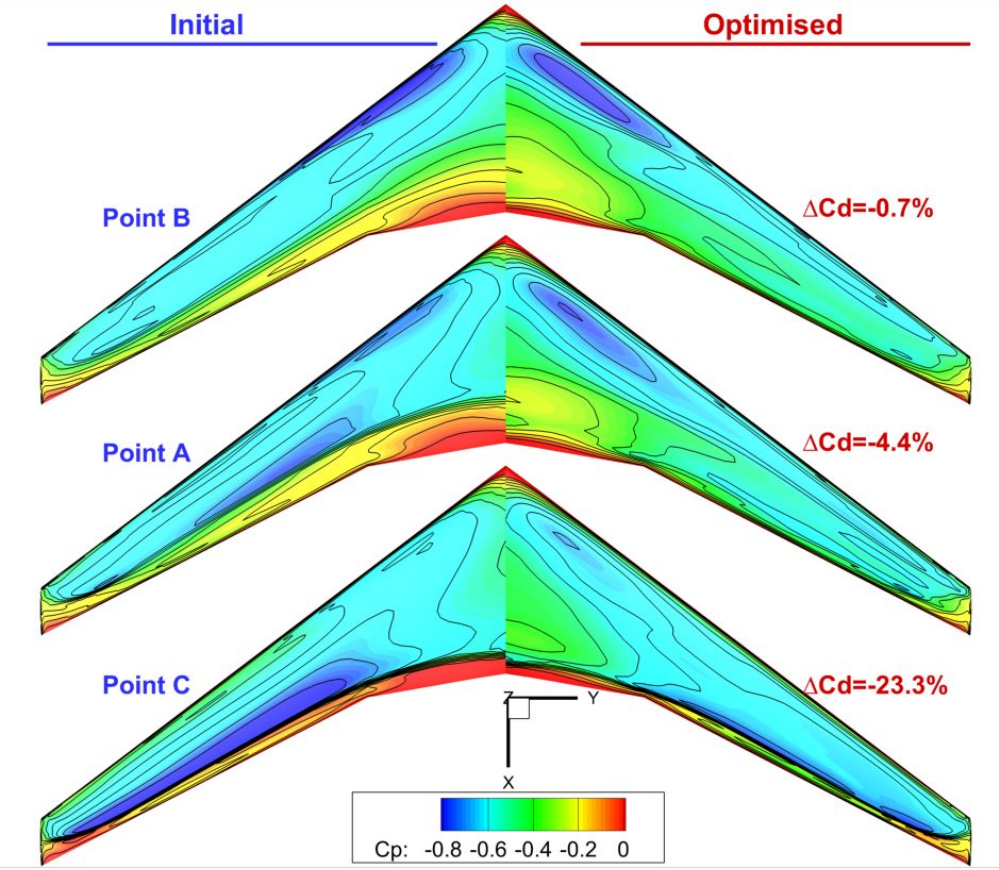

Figure 7: Surface C_P of initial and optimized geometry for case 4.4

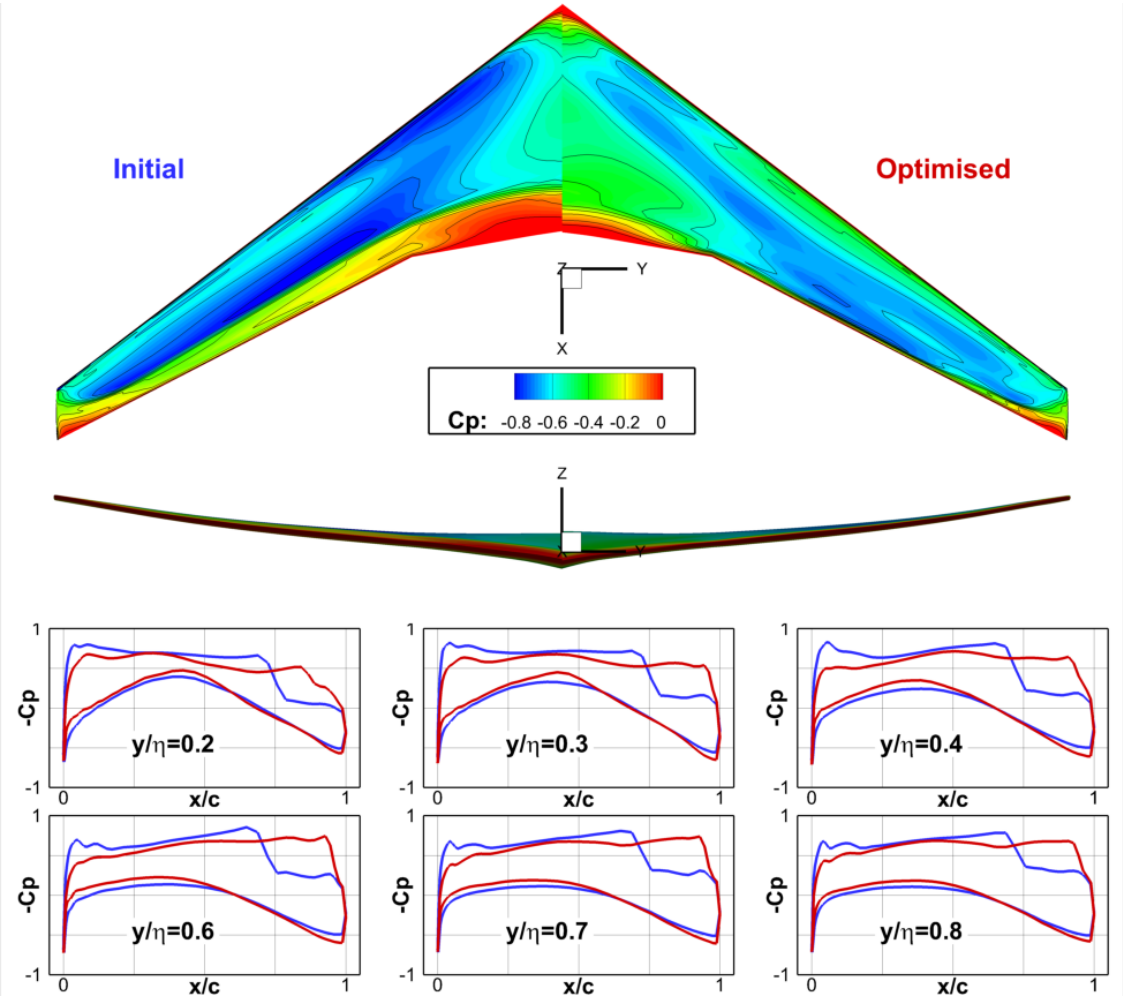

Figure 8: Surface C_P of initial and optimized geometry for range at $l = 0.40$

VI. Conclusions and Ongoing Work

A study into the effect of the choice of optimization problem for aerodynamic shape optimization has been presented. The Breguet range parameter has been considered with the design point also being a variable. The Mach number is allowed to vary, hence a non-dimensional measure of wing loading needs to be introduced as a constraint. This problem is also more indicative of an aircraft objective than drag minimization and is equivalent in cost to a single-point optimization.

Previous work by the authors has studied the effect that the optimization problem has on aerofoil problems. It has been shown that a shocked, optimal solution can be found when performing range optimization. Hence, in this work this problem has been studied for full wing optimization. An analytical treatment has demonstrated that compared to not including three-dimensional drag effects, range optimization results in higher optimum Mach numbers with lower corresponding lift coefficients. Full optimizations of the NASA CRM wing have been performed, including a single- and multi-point case each based on the AIAA ADODG cases. Shock-free solutions are found for the single-point case and at a number of the multi-point cases. However, range optimization results in a shocked solution.

References

[1]Hicks, R. M. and Henne, P. A., "Wing Design by Numerical Optimization," *Journal of Aircraft*, Vol. 15, No. 7, 1978, pp. 407–412.
doi:10.2514/6.1977-1247.

[2]Qin, N., Vavalle, A., Le Moigne, A., Laban, M., Hackett, K., and Weinerfelt, P., "Aerodynamic Considerations of Blended Wing Body Aircraft," *Progress in Aerospace Sciences*, Vol. 40, No. 6, 2004, pp. 321–343.
doi:10.1016/j.paerosci.2004.08.001.

[3]Nielsen, E. J., Lee-Rausch, E. M., and Jones, W. T., "Adjoint Based Design of Rotors in a Noninertial Frame," *Journal of Aircraft*, Vol. 47, No. 2, 2010, pp. 638–646.
doi:10.2514/1.46044.

[4]Lyu, Z., Kenway, G. K. W., and Martins, J. R. R. A., "Aerodynamic Shape Optimization Investigations of the Common Research Model Wing Benchmark," *AIAA Journal*, Vol. 53, No. 4, 2015, pp. 968–985.
doi:10.2514/1.J053318.

[5]Choi, S., Lee, K. H., Potsdam, M., and Alonso, J. J., "Helicopter Rotor Design Using a Time-Spectral and Adjoint Based Method," *Journal of Aircraft*, Vol. 51, No. 2, 2014, pp. 412–423.
doi:10.2514/1.C031975.

[6]Morris, A. M., Allen, C. B., and Rendall, T. C. S., "CFD-based Optimization of Aerofoils Using Radial Basis Functions for Domain Element Parameterization and Mesh Deformation," *International Journal for Numerical Methods in Fluids*, Vol. 58, No. 8, 2008, pp. 827–860.
doi:10.1002/fld.1769.

[7]Poole, D. J., Allen, C. B., and Rendall, T. C. S., "High-fidelity aerodynamic shape optimization using efficient orthogonal modal design variables with a constrained global optimizer," *Computers & Fluids*, Vol. 143, 2017, pp. 1–15.
doi:10.1016/j.compfluid.2016.11.002.

[8]Masters, D. A., Taylor, N. J., Rendall, T. C. S., and Allen, C. B., "Multilevel Subdivision Parameterization Scheme for Aerodynamic Shape Optimization," *AIAA Journal*, Vol. 55, No. 10, 2017, pp. 3288–3303.
doi:10.2514/1.J055785.

[9]Kedward, L. J., Allen, C. B., and Rendall, T. C. S., "Gradient-Limiting Shape Control for Efficient Aerodynamic Optimisation," *AIAA Aviation 2018 Forum*, Dallas, Texas, 2018, AIAA Paperr 2018-3951.
doi:10.2514/6.2018-3951.

[10]Boerstoel, J., "A Survey of Symmetrical Transonic Potential Flows around Quasi-elliptical Aerofoil Sections," Tech. rep., NLR, 1967, NLR Report TR.T179.

[11]Nieuwland, G., "Transonic Potential Flow around a Family of Quasi-elliptical Aerofoil Sections," Tech. rep., NLR, 1967, NLR Report TR.T172.

[12]Harbeck, M. and Jameson, A., "Exploring the Limits of Transonic Shock-free Airfoil Design," *43rd AIAA Aerospace Sciences Meeting and Exhibit*, Reno, Nevada, 2005, AIAA Paper 2005-1041.
doi:10.2514/6.2005-1041.

[13]Carrier, G., Destarac, D., Dumont, A., Meheut, M., Salah El Din, I., Peter, J., Ben Khelil, S., Brezillon, J., and Pestana, M., "Gradient-Based Aerodynamic Optimization with the elsA Software," *52nd AIAA Aerospace Sciences Meeting*, National Harbor, Maryland, 2014, AIAA Paper 2014-0568.
doi:10.2514/6.2014-0568.

[14]Bisson, F., Nadarajah, S. K., and Shi-Dong, D., "Adjoint-Based Aerodynamic Optimization Framework," *52nd AIAA Aerospace Sciences Meeting*, National Harbor, Maryland, 2014, AIAA Paper 2014-0412.
doi:10.2514/6.2014-0412.

[15]Poole, D. J., Allen, C. B., and Rendall, T. C. S., "Control Point-Based Aerodynamic Shape Optimization Applied to AIAA ADODG Test Cases," *53rd AIAA Aerospace Sciences Meeting*, Kissimmee, Florida, 2015, AIAA Paper 2015-1947.
doi:10.2514/6.2015-1947.

[16]LeDoux, S. T., Vassberg, J. C., Young, D. P., Fugal, S., Kamenetskiy, D., Huffman, W. P., Melvin, R. G., and Smith, M. F., "Study Based on the AIAA Aerodynamic Design Optimization Discussion Group Test Cases," *AIAA Journal*, Vol. 53, No. 7, 2015, pp. 1910–1935.
doi:10.2514/1.J053535.

[17]Lee, C., Koo, D., Telidetzki, K., Buckley, H. P., Gagnon, H., and Zingg, D. W., "Aerodynamic Shape Optimization of Benchmark Problems Using Jetstream," *53rd AIAA Aerospace Sciences Meeting*, Orlando, Florida, 2015, AIAA Paper 2015-0262.
doi:10.2514/6.2015-0262.

[18]Morawetz, C. S., "On the non-existence of continuous transonic flows past profiles III," *Communications on Pure and Applied Mathematics*, Vol. 11, No. 1, 1958, pp. 129–144.
doi:10.1002/cpa.3160110107.

[19]Jameson, A., Vassberg, J. C., and Ou, K., "Further Studies of Airfoils Supporting Non-Unique Solutions in Transonic Flow," *AIAA Journal*, Vol. 50, No. 12, 2012, pp. 2865–2881.
doi:10.2514/1.J051713.

[20]Harris, C. D., "NASA Supercritical Airfoils: A Matrix of Family-Related Airfoils," Tech. rep., Langley Research Center, Hampton, Virginia, 1990, NASA Technical Paper 2969.

[21]Epstein, B., Jameson, A., Peigin, S., Roman, D., Harrison, N., and Vassberg, J., "Comparative Study of Three-Dimensional Wing Drag Minimization by Different Optimization Techniques," *Journal of Aircraft*, Vol. 46, No. 2, 2009, pp. 526–541.
doi:10.2514/1.38216.

[22]Buckley, H. P., Zhou, B. Y., and Zingg, D. W., "Airfoil Optimization Using Practical Aerodynamic Design Requirements," *Journal of Aircraft*, Vol. 47, No. 5, 2010, pp. 1707–1719.
doi:10.2514/1.C000256.

[23]Zingg, D. W. and Elias, S., "Aerodynamic Optimization Under a Range of Operating Conditions," *AIAA Journal*, Vol. 44, No. 11, 2006, pp. 2787–2792.
doi:10.2514/1.23658.

[24]Liem, R. P., Kenway, G. K. W., and Martins, J. R. R. A., "Multimission Aircraft Fuel-Burn Minimization via Multipoint Aerostructural Optimization," *AIAA Journal*, Vol. 53, No. 1, 2015, pp. 104–122.
doi:10.2514/1.J052940.

[25]Drela, M., "Pros and Cons of Airfoil Optimization," in Caughey, D. and Hafez, M., eds., "Frontiers of Computational Fluid Dynamics," World Scientific, pp. 363–381, 1998.
doi:10.1142/9789812815774_0019.

[26]Doherty, J. J., "Transonic Airfoil Study Using Sonic Plateau, Optimization and Off-Design Performance Maps," *35th AIAA Applied Aerodynamics Conference*, Denver, Colorado, 2017, AIAA Paper 2017-3056.
doi:10.2514/6.2017-3056.

[27]Poole, D. J., Allen, C. B., and Rendall, T. C. S., "Comparison of Point Design and Range-Based Objectives for Transonic Aerofoil Optimization," *AIAA Journal*, Vol. 56, No. 8, 2018, pp. 3240–3256.
doi:10.2514/1.J056627.

[28]Mair, W. A. and Birdsall, D. L., *Aircraft Performance*, Cambridge University Press, 1992.

[29]Hanke, C. R. and Nordwall, D. R., "The Simulation of a Jumbo Jet Transport Aircraft. Volume 2: Modeling Data," Tech. rep., NASA, 1970, NASA-CR-114494.

[30]Buckley, H. P. and Zingg, D. W., "Approach to Aerodynamic Design Through Numerical Optimization," *AIAA Journal*, Vol. 51, No. 8, 2013, pp. 1972–1981.
doi:10.2514/1.J052268.

[31]Lock, C. N. H., "The Ideal Drag Due to a Shock Wave Parts I and II," Tech. rep., Aeronautical Research Council, 1951, ARC report 2512.

[32]Poole, D. J., Allen, C. B., and Rendall, T. C. S., "Metric-Based Mathematical Derivation of Efficient Airfoil Design Variables," *AIAA Journal*, Vol. 53, No. 5, 2015, pp. 1349–1361.
doi:10.2514/1.J053427.

[33]Rendall, T. C. S. and Allen, C. B., "Unified Fluid-Structure Interpolation and Mesh Motion Using Radial Basis Functions," *International Journal for Numerical Methods in Engineering*, Vol. 74, No. 10, 2008, pp. 1519–1559.
doi:10.1002/nme.2219.

[34]Wendland, H., *Scattered Data Approximation*, Cambridge University Press, 1st ed., 2005.

[35]Allen, C. B., Poole, D. J., and Rendall, T. C. S., "Wing aerodynamic optimization using efficient mathematically-extracted modal design variables," *Optimization and Engineering*, Vol. 19, No. 2, 2018, pp. 453–477.
doi:10.1007/s11081-018-9376-7.

[36]Yu, Y., Lyu, Z., Xu, Z., and Martins, J. R. R. A., "On the influence of optimization algorithm and initial design on wing aerodynamic shape optimization," *Aerospace Science and Technology*, Vol. 75, 2018, pp. 183–199.
doi:10.1016/j.ast.2018.01.016.

[37]Zhou, J. L., Tits, A. L., and Lawrence, C. T., "Users Guide for FSQP Version 3.7 : A Fortran Code for Solving Optimization Programs, Possibly Minimax, with General Inequality Constraints and Linear Equality Constraints, Generating Feasible Iterates," Tech. rep., Institute for Systems Research, University of Maryland, 1997, SRC-TR-92-107r5.

[38]Mayne, D. Q. and Polack, E., "A surperlinearly convergent algorithm for constrained optimization problems," *Mathematical Programming Studies*, Vol. 4, 1982, pp. 45–61.
doi:10.1007/BFb0120947.

[39]Grippo, L., Lampariello, F., and Lucidi, S., "A Nonmonotone Line Search Technique for Newton's Method," *SIAM Journal on Numerical Analysis*, Vol. 23, No. 4, 1986, pp. 707–716.
doi:10.1137/0723046.

[40]Panier, E. R. and Tits, A. L., "Avoiding the Maratos Effect by Means of a Nonmonotone Line Search I. General Constrained Problems," *SIAM Journal on Numerical Analysis*, Vol. 28, No. 4, 1991, pp. 1183–1195.
doi:10.1137/0728063.

[41]Bonnans, J. F., Panier, E. R., Tits, A. L., and Zhou, J. L., "Avoiding the Maratos Effect by Means of a Nonmonotone Line Search II. Inequality Constrained Problems–Feasible Iterates," *SIAM Journal on Numerical Analysis*, Vol. 29, No. 4, 1992, pp. 1187–1202.
doi:10.1137/0729072.

[42]van Leer, B., "Flux-vector splitting for the Euler equations," *Eighth International Conference on Numerical Methods in Fluid Dynamics*, Lecture Notes in Physics, 1982, pp. 507–512.
doi:10.1007/3-540-11948-5_66.

[43]Allen, C. B., "Multigrid Acceleration of an Upwind Euler Method for Hovering Rotor Flows," *The Aeronautical Journal*, Vol. 105, No. 1051, 2001, pp. 517–524.
doi:10.1017/S0001924000017954.

[44]Allen, C. B., "Towards Automatic Structured Multiblock Mesh Generation using Improved Transfinite Interpolation," *International Journal for Numerical Methods in Engineering*, Vol. 74, No. 5, 2008, pp. 697–733.
doi:10.1002/nme.2170.